Solution Structure and Interdomain Interactions of the *Saccharomyces cerevisiae* "TATA Binding Protein" (TBP) Probed by Radiolytic Protein Footprinting†

Hassan Rashidzadeh,‡,§,|| Sergei Khrapunov,⊥ Mark R. Chance,‡,§,⊥ and Michael Brenowitz*,§,⊥

Departments of Biochemistry and of Physiology and Biophysics and Center for Synchrotron Biosciences, Albert Einstein College of Medicine, 1300 Morris Park Avenue, Bronx, New York 10461

Received November 20, 2002; Revised Manuscript Received February 14, 2003

ABSTRACT: Although atomic-resolution crystal structures of the conserved C-terminal domain of several species of TBP and their complexes with DNA have been determined, little information is available concerning the structure in solution of full-length TBP containing both the conserved C-terminal and nonconserved N-terminal domains. Quantitation of the amino acid side chain oxidation products generated by synchrotron X-ray radiolysis by mass spectrometry has been used to determine the solvent accessibility of individual residues in monomeric *Saccharomyces cerevisiae* TATA binding protein (TBP) free in solution and in the TBP−DNA complex. Amino acid side chains within the C-terminal domain of unliganded full-length TBP that are predicted to be accessible from crystal structures of the isolated domain are protected from oxidation. Residues within the N-terminal domain are also protected from oxidation in both the absence and presence of DNA. Some residues within the DNA-binding "saddle" of the C-terminal domain are protected upon formation of a TBP−DNA complex as expected, while others are protected in both the absence and presence of bound DNA. In addition, residues on the upper side of the β-sheets undergo reactivity changes as a function of DNA binding. These data suggest that the DNA-binding saddle of monomeric unliganded yeast TBP is only partially accessible to solvent, the N-terminal domain is partially structured, and the N- and C-terminal domains form a different set of contacts in the free and DNA-bound protein. The functional implications of these results are discussed.

The selection of the RNA polymerase by which genes in eukaryotic organisms are transcribed is the result of the assembly on promoters of proteins called "transcription factors" (TFs)[1] that are specific to each of the three RNA polymerases. The "TATA box binding protein" (TBP) is a component of the nucleoprotein complexes required for the initiation of transcription by each of the three eukaryotic RNA polymerases (*1*). TBP binds with high affinity and specificity to DNA with a consensus sequence of TATAa/tAa/t (*2*) while introducing a dramatic and unusual bend to the bound DNA (*3*−*8*) that is dependent on the TATA sequence (*9*−*11*) and solution condition (*12*). The ability of TBP to form complexes with the additional transcription factors required to specify RNA polymerase I, II, or III (*13*−*15*) is a key feature of its biological function. Last, TBP has been shown to self-associate *in vitro*. A monomer−tetramer−octamer equilibrium has been demonstrated for *Saccharomyces cerevisiae* TBP that is highly dependent upon solution conditions (*16*−*18*). *S. cerevisiae* TBP forms dimers under different solution conditions, including the presence of a specific nonionic detergent (*19*) or upon deletion of its N-terminal domain (*18*).

TBP molecules from all eukaryotic species possess two domains. The C-terminal domain is highly conserved and both necessary and sufficient for DNA sequence specific binding by TBP as well as preinitiation complex (PIC) assembly (*20*, *21*). In contrast, the N-terminal domain is far less conserved and differs significantly in length among eukaryotes (*22*). The crystal structures that have been determined for free TBP (*23*, *24*), TBP−DNA complexes (*3*, *4*, *6*−*8*), and ternary complexes of TBP with other transcription factors (*25*−*28*) provide an extensive and detailed understanding of the structure of the C-terminal domain and its complexes with DNA and other transcription proteins. However, these structures of C-terminal domains have N-terminal domains that are either rudimentary (i.e., *Arabidopsis thaliana*) or deleted. Thus, the structures of N-terminal domains are poorly understood.

Evidence for functional roles of the N-terminal domain of TBP in transcriptional regulation is beginning to emerge. The epitope of a monoclonal antibody that inhibits transcription by polymerases II and III *in vitro* (*29*) is within the N-terminal domain of human TBP. The N-terminal domain of human TBP mediates interaction with HMG-1 (*30*), downregulates binding to the U6 TATA box, mediates cooperative binding with the SNAPc complex, and enhances transcription (*31*). The presence of the N-terminal domain

† This work was supported by NIH Grants GM-39929, CA-84713, and RR-01633.

* To whom correspondence should be addressed. E-mail: brenowit@aecom.yu.edu. Phone: (718) 430-3179. Fax: (718) 430-8565.

‡ Department of Physiology and Biophysics.

§ Center for Synchrotron Biosciences.

|| Present address: Biolytics Corp., 4250 Route 1, Monmouth Junction, NJ 08852.

⊥ Department of Biochemistry.

[1] Abbreviations: TFs, transcription factors; TATAAAAG, 5′-TATAAAAG-3′; TBP, TATA binding protein; RY, 5′-purine-pyrimidine-3′; YR, 5′-pyrimidine-purine-3′; NSLS, National Synchrotron Light Source; FRET, fluorescence resonance energy transfer.

10.1021/bi027203f CCC: $25.00
Published on Web 03/15/2003

of human TBP inhibits DNA binding *in vitro*; mutations within the C-terminal domain outside the DNA-binding saddle can relieve this inhibition (*32*). The N-terminal domain of *S. cerevisiae* TBP is also reported to destabilize its complex with DNA (*20*, *33*). Although yeast cells in which the DNA encoding the N-terminal domain has been deleted are viable, genetic studies have shown that deletion of the N-terminal domain is lethal in conjunction with specific TBP C-terminal domain mutations that are by themselves not deleterious (*34*). The N-terminal domain mediates the self-association of *S. cerevisiae* TBP into tetramers and octamers (*17*), and its absence favors formation of dimers (*18*).

A "footprinting" method has been developed that utilizes millisecond exposure of protein solutions to a synchrotron X-ray beam to produce hydroxyl radicals (•OH) by radiolysis. The side chains of amino acids Cys, Met, Phe, Tyr, Trp, Pro, His, and Leu are preferentially oxidized; mass spectrometry is used to quantitate the radiolytic reaction products (*35*). The analysis of the rates of radiolytic modification allows the correlation of reactivity with the solvent accessibility of the side chain residue (*36*−*38*). This approach is now applied to the structure in solution of full-length monomeric *S. cerevisiae* TBP and monomeric TBP complexed to DNA bearing a high-affinity TATA box. The results of these studies reveal a number of unexpected structural features of yeast TBP that are consistent with the conclusions drawn from a complementary intrinsic fluorescence analysis (*39*).

EXPERIMENTAL PROCEDURES

Materials

The *S. cerevisiae* TBP used in these studies was expressed in *Escherichia coli* and purified as described previously (*40*, *41*). This protein is fully active in sequence specific DNA binding (see Results). Aliquots of protein were removed from a −70 °C storage solution and diluted to a concentration of 0.7 μM in "assay buffer" [10 mM sodium cacodylate (Sigma) and 120 mM KCl (pH 7.4)] prior to exposure to the synchrotron X-ray beam. An extinction coefficient of 13.4 $\times$ 10^3 M^{-1} cm^{-1} was used to calculate the TBP concentration. The dilute protein samples were incubated at room temperature for 20−30 min prior to exposure to the X-ray beam. Mass spectral analysis shows that the N-terminal methionine of *S. cerevisiae* TBP is not present in the bacterially expressed protein (data not shown). However, the numbering of the residues in this paper commences with this methionine for consistency with the published literature.

An HPLC-purified 14-base oligonucleotide with a 5′-CGC**TATAAAAG**GGC-3′ sequence and its complement were purchased from TriLink Bio Technologies Inc. (San Diego, CA) and used without further purification. The concentration of oligonucleotides was determined using extinction coefficients calculated from the known base pair composition. A duplex of these oligonucleotides was prepared by mixing equimolar amounts of the oligonucleotide and its complement in assay buffer and allowing them to anneal for 1 h at room temperature. The efficiency of duplex formation was monitored using fluorescence resonance energy transfer (*39*, *41*) by annealing top and bottom strand oligonucleotides of the same sequences separately labeled with fluorescein (donor) and TAMRA (acceptor), respectively.

A complex of TBP with the 14 bp DNA duplex was prepared by mixing 0.7 μM TBP with a 2-fold molar excess of DNA. The protein and DNA were allowed to equilibrate for 25−30 min at room temperature prior to X-ray exposure.

Methods

Synchrotron Footprinting. Samples were exposed to the white light X-ray beam of NSLS beamline X-28C at the Brookhaven National Laboratory (Upton, NY). Experiments were conducted at a ring energy of 2.8 GeV and beam currents between 180 and 220 mA. Detailed descriptions of the beamline and the apparatus used in these experiments have been published (*42*−*44*). The quench-flow mixer (KinTek, State College, PA) used at the beamline was modified so that a single syringe pushed sample from loops of either 200 or 400 μL through the X-ray beam. The flow rate of the sample past the X-ray beam was adjusted to control the exposure time. This continuous flow mode allowed large volumes of low-concentration samples to be exposed to the X-ray beam for 30−100 ms and collected. A temperature of 22 °C was maintained by a circulating water bath. Collected samples were frozen at −20 °C immediately following an experiment for transport back to the laboratory for mass spectrometric analysis.

Protein Activity Determination. The activity of the TBP preparation used in this study was obtained by a novel intrinsic protein fluorescence assay that takes advantage of the tyrosine fluorescence quenching and tryptophan fluorescence enhancement that occurs upon formation of the TBP−DNA complex (*39*). TBP at 1 μM was titrated with the 14 bp oligonucleotide in assay buffer at 22 °C. This protein concentration is above the K_d of binding for this DNA sequence and thus is stoichiometric under these experimental conditions. The fluorescence of the solutions was measured at 306 nm (tyrosine fluorescence) and 365 nm (tryptophan fluorescence) following excitation at 275 nm. The inner filter effect due to the changing DNA concentration was avoided by using a common excitation wavelength of 275 nm. The 310 nm/365 nm fluorescence ratio was plotted versus DNA concentration. The fractional activity of the TBP preparation was obtained by least-squares fitting using a function that determines the intersection of two lines.

Chromatography and Mass Spectrometry. The frozen samples were thawed, and either trypsin (Promega) or chymotrypsin (Roche) was added to an enzyme:protein ratio of 1:50 (w/w).[2] The samples were incubated at 37 °C for 12 h and introduced into the ion source via a Waters Alliance 2690 high-pressure liquid chromatography system (Waters Corp., Milford, MA). Reverse-phase chromatographic separation was performed on a 1 mm $\times$ 150 mm C18 column (Vydac Separations Group Inc., Hesperia, CA) at a flow rate of 50 μL/min and a 2% gradient of acetonitrile and water containing 0.05% trifluoroacetic acid.

[2] Trypsin digestion is a preferred procedure since the resultant peptides contain Arg or Lys at the carboxyl terminus. The amine present on these side chains improves the efficiency of ionization during mass spectrometry. Only peptide 182−194 was obtained by chymotrypsin digestion in these studies.

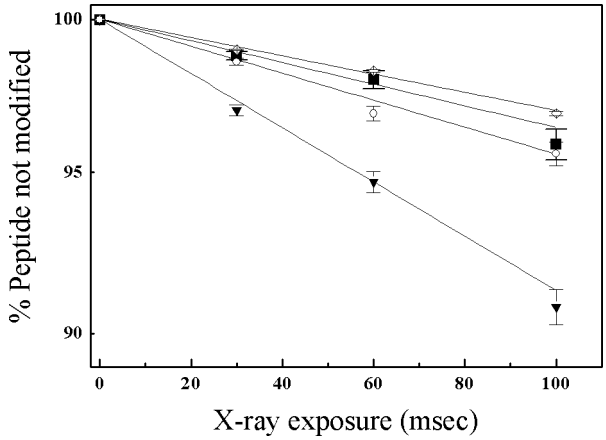

FIGURE 1: Dose−response profiles for the radiolytic modification of peptide 84−90 [(▼) 0.32 ± 0.02 s^{-1}], peptide 111−120 [(○) 0.37 ± 0.04 s^{-1}], peptide 146−151 [(■) 0.39 ± 0.07 s^{-1}], and peptide 183−195 [(◇) 0.86 ± 0.03 s^{-1}] derived from free TBP.

Mass spectrometry data were acquired using a quadrupole ion trap mass spectrometer (ThermoFinnigan LCQ, ThermoFinnigan Inc., San Jose, CA) equipped with an electrospray ion source. Both ESI mass spectra and MS/MS spectra of the proteolytic peptides were recorded in the centroid mode. Nitrogen was used as the nebulizer gas with a needle voltage of 4.5 kV (*35*). The fractions of modified peptides were determined from the ratio of the area under ion signals for the radiolytic products to the sum of those for the unoxidized peptides and the radiolytic products (*35*−*37*). The fraction peptide modified versus exposure time (a "dose−response" plot) was fit to an exponential decay function within Origin version 6.1 (OriginLabs) to determine the rate of peptide modification.

Solvent Accessibility Calculations. The solvent accessibilities of individual residues within the C-terminal domain of *S. cerevisiae* TBP in the absence of DNA were determined for a single monomer extracted from the 1TBP crystal structure (*24*). Solvent accessibility calculations for the C-terminal domain−DNA complex were determined from the 1YTB crystal structure (*4*). The program GETAREA 1.1 (http://www.scsb.utmb.edu/cgi-bin/get_a_form.tcl) was used to calculate the solvent accessible surface area per residue and per atom from the PDB files.

TBP Models. The pictures in Figure 6 were created by adding the 61 residues of the N-terminal domain to the structure of 1TBP and 1YTB in the Swiss PDB viewer program (*48*) and manually adjusting the torsion angles of the polypeptide backbone. No refinement or minimization was used in generating these representations.

RESULTS

The studies of unliganded TBP were conducted under solution conditions and protein concentrations such that TBP was entirely monomeric (refs *16* and *17* and data not shown). Figure 1 shows the loss of the unmodified fraction as a function of X-ray beam exposure for various TBP peptides that were generated by digestion of TBP samples exposed to the beam for periods ranging from 30 to 100 ms. The fraction unmodified for the specific peptides determined by quantitation of the LC-coupled mass spectrometry data is expressed as the ratio of the unmodified ions to the total [i.e., modified plus unmodified ions (*35*−*38*)]. Unlike •OH footprinting of nucleic acids in which all the backbone positions display comparable reactivities, the amino acid side chains are differentially reactive to •OH (*35*). Thus, in the analysis that follows, we will focus on the relative rates of like side chains and the effect of DNA binding on reactivity. The modification rates obtained for residues within the C-terminal domain are compared with the solvent accessibilities calculated from a single monomer extracted from the free and DNA-bound crystal structures of this domain (Figure 2). Although these comparisons are limited by the absence of the N-terminal domain in these structures, as will be shown below, they provide a valuable guide through the data.

Stoichiometric Titration. In the comparison of the reactivity to •OH modification of TBP residues in the presence and absence of DNA, it was essential to establish that the protein preparation used in this study was fully active in DNA binding. Figure 3 shows the results of a stoichiometric titration of TBP by the oligonucleotide bearing the high-affinity binding sequence TATAAAAG. The fluorescence difference spectrum (Figure 3, inset) displays two maxima. These maxima are due to quenching of the fluorescence of the tyrosine residues within the C-terminal domain and the increase in the fluorescence of the tryptophan residue located within the N-terminal domain upon the binding of DNA to TBP (*39*). The ratio of tryptophan and tyrosine fluorescence intensities increases with increasing DNA concentration and yields a protein:DNA stoichiometry of 0.95−1.0 (Figure 3). Thus, essentially all the protein is complexed at the 2-fold molar excess of DNA present in the radiolytic experiments.

H2 Subdomain of the C-Terminal Domain. The two subdomains of the C-terminal domain of *S. cerevisiae* TBP will be called by the names of the helices that grace their upper surface, H2 and H2′. The peptides containing residues 111−120 and 84−90 are located within the H2 subdomain. The reactive residues of the first peptide are located within the DNA-binding saddle, while the latter are on the top of the molecule; peptide 111−120 contains one of the phenylalanine residues that stabilize the protein-induced DNA kink (Figure 2A). The reactivity of this peptide is low (0.37 ± 0.04 s^{-1}) and dominated by F116 by virtue of the greater intrinsic •OH reactivity of phenylalanine relative to leucine (Figures 1 and 2A).

The low reactivity of peptide 111−120 in the absence of DNA was surprising given the high calculated solvent accessibility of F116 and L114 (∼41 and ∼64 $Å^2$, respectively) in the isolated C-terminal domain in the absence of DNA. As a reference, a phenylalanine residue on the surface of lysozyme with a calculated solvent accessibility of 40.3 Å is oxidized under comparable conditions at a rate of 3.3 ± 0.1 s^{-1} (*45*). As will be seen below, phenylalanine oxidation rates of ∼3 s^{-1} are typical for solvent accessible residues in our synchrotron footprinting experiments. The reactivity of this peptide is diminished by less than 25% upon the binding of DNA. The solvent accessibility calculation indicates complete burial of F116 and L114 from solvent (Figure 2A). These results suggest that these side chains are solvent inaccessible in *both* the absence and presence of bound DNA.

The surprises continue with consideration of peptide 84−90. The low reactivity of L87 and H88 might be ascribed to

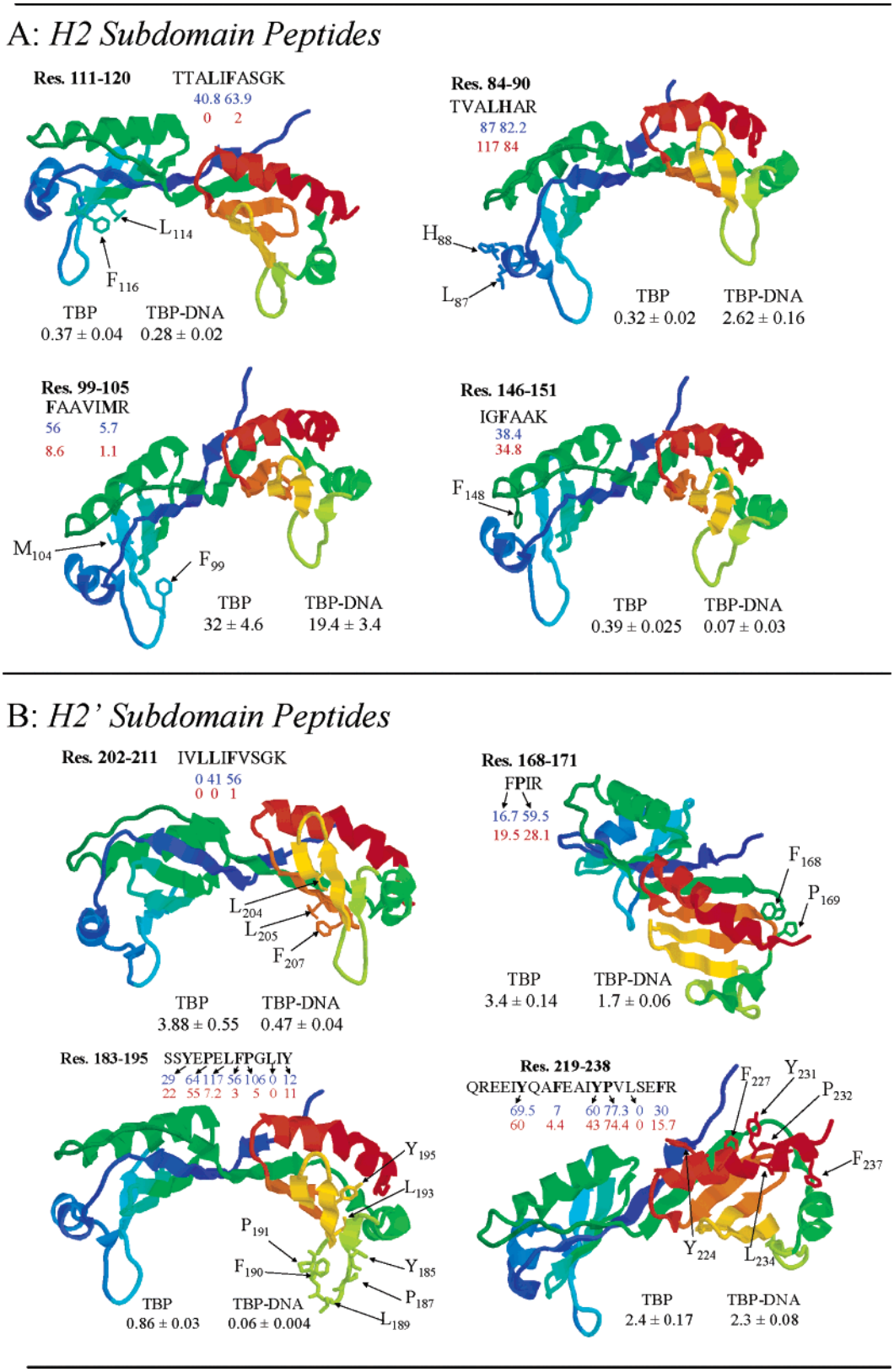

FIGURE 2: Ribbon diagram representations of the C-terminal domain of *S. cerevisiae* TBP in which radiolytically modified residues are denoted. The values denoted TBP and TBP-DNA included in each panel are the rates of peptide modification (in units of inverse seconds) determined from data such as that shown in Figure 1. The solvent accessibility of the modifiable residues in square angstroms calculated from the crystal and cocrystal structures of the C-terminal domain of TBP are displayed underneath the residue sequence in blue for the C-terminal domain of TBP and red for the C-terminal domain of TBP complexed with DNA.

the lower intrinsic •OH modification rates of these side chains (compared with phenylalanine) in light of their high solvent accessibility in the C-terminal core. However, their reactivity *increases* by almost 10-fold in the TBP−DNA complex despite little change in their calculated solvent accessibility (Figures 1 and 2A). These results suggest that L87 and H88 are protected in the absence but not in the presence of DNA.

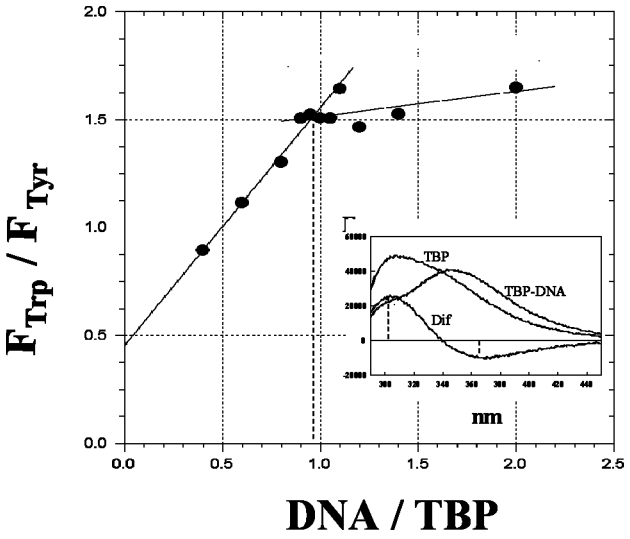

FIGURE 3: Determination of the DNA binding activity of the *S. cerevisiae* TBP used in these experiments. The ratio of the fluorescence emissions at 365 nm (F_{Trp}) and 306 nm (F_{Tyr}) obtained using an excitation wavelength of 275 nm of a solution containing 1.0 μM TBP was monitored as a function of the concentration of an oligonucleotide bearing the high-affinity sequence TATAAAAG. The data were fit to two intersecting lines. The fractional activity of the protein (assuming the well-documented 1:1 stoichiometry of this TBP−DNA complex) was determined from intersection. The insert presents the fluorescence emission spectra of TBP in the absence (TBP) and presence of DNA at a 1:1 protein:DNA ratio (TBP−DNA). The difference spectrum (Dif) was obtained by subtraction of the TBP−DNA spectrum from the TBP spectrum (TBP). The wavelengths at which the ratio of tryptophan (365 nm) and tyrosine (306 nm) fluorescence was measured are shown by the dotted lines.

The peptide comprising residues 99−105 contains a highly oxidizable methionine (*35*), resulting in a very high modification rate of 32 ± 4.6 s^{-1} for this peptide (Figure 2A). Methionine residues display a problematic relationship between oxidation rate and solvent accessibility; it has been suggested that the oxidation of methionine residues in synchrotron radiolysis is a combination of their accessibility and their sensitivity to intramolecular electron transfer (*45*). To specifically probe F99, the other phenylalanine residue on the H2 subdomain stirrup involved in stabilizing the DNA kink, MS/MS fragmentation was performed on this oxidized peptide to determine the site(s) of oxidation. Figure 4 shows the MS/MS spectrum of the singly oxidized radiolytic product of this peptide. This spectrum shows that the b_2−b_5 ions are not +16 mass units heavier like those that would result from F99 oxidation. In contrast, +16 ions of b_6 and y_2 are substantially present in the spectrum, consistent with oxidation of M104. These data qualitatively indicate that F99 is not significantly oxidized in this peptide, consistent with the limited reactivity of F116 and L114 (peptide 111−120) within this side of the DNA-binding saddle. Although this peptide displays a reduction in reactivity upon formation of the TBP−DNA complex, the problematic behavior of methionine side chains to •OH modification precludes definitive interpretation of this result.

Peptide 146−151 contains a single reactive residue, F148, on helix 2, on the back of the C-terminal domain (Figures 1A and 2A). Despite the intrinsic radiolytic sensitivity of phenylalanine and the calculated high accessibility of this residue, F148 is characterized by low reactivity in the absence

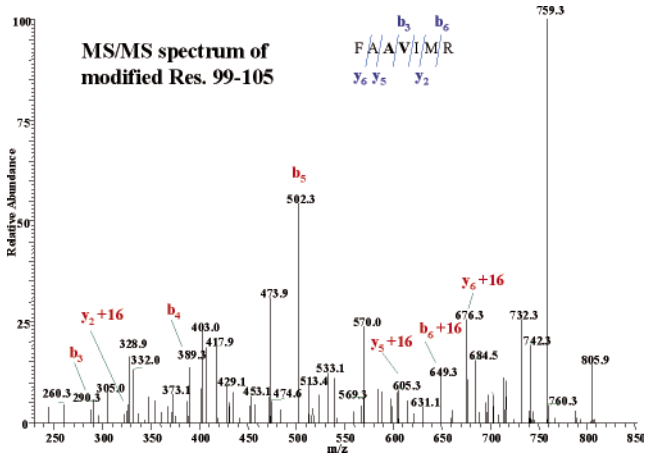

FIGURE 4: ESI-MS/MS tandem mass spectrum of singly oxidized residues 99−105 from exposure of the protein to the X-ray beam at 30 ms.

of DNA that is further diminished upon DNA binding (0.39 ± 0.03 and 0.07 ± 0.03 s^{-1}, respectively). As noted above, oxidation rates of ~3 s^{-1} are typically observed for solvent-exposed phenylalanine residues (*45*).

Two conclusions can be drawn from this aggregate of results for the H2 subdomain of full-length TBP (Figure 2A). First, the half of the DNA-binding saddle formed by the H2 subdomain is effectively protected from solvent in *both* the absence and presence of DNA. Second, the residues away from the DNA-binding saddle display reactivities that are sensitive to DNA binding and inconsistent with the accessibilities calculated from the C-terminal core structures.

H2′ Subdomain of the C-Terminal Domain. Two questions are central as we continue through the reactive residues within the H2′ subdomain. First, are residue reactivities symmetry-related? Second, are residue reactivities consistent with the available structural information? Peptide 202−211 contains three reactive residues lining the DNA-binding saddle, of which two are predicted to be accessible in the absence of DNA and completely buried in its presence (Figures 1 and 2B). The third residue (L205) is predicted to be inaccessible in both cases. This peptide is highly reactive in the free protein and protected by almost 10-fold in the TBP−DNA complex. The high intrinsic reactivity of phenylalanine is again expected to dominate the measured reactivity of this peptide. The rate of reactivity for this peptide (3.88 ± 0.55 s^{-1}) is comparable to the standard (~3 s^{-1}) for highly solvent accessible phenylalanine residues (*45*).

Similar 10-fold protection is observed for peptide 183−195 that contains three reactive residues (L189, F190, and P191) that are buried upon formation of the TBP−DNA complex (Figures 1 and 2B). Since this peptide contains a large number of reactive residues, it is not a spatially precise probe. However, all of the reactive residues are in the H2′ subdomain, thus rendering this peptide a useful probe at the subdomain level. Thus, *asymmetry* in the •OH reactivity is evident across the 2-fold symmetry axis of TBP; the two sides of the DNA-binding saddle of *monomeric* TBP are not equally solvent accessible in the absence of DNA, while the saddle residues of the H2′ subdomain are reactive in the absence of DNA and protected in its presence.

This asymmetry to •OH reactivity relative to the protein's 2-fold symmetry axis extends to the top surface of TBP.

Peptide 168−171 contains two reactive residues that are solvent-exposed away from the saddle (Figure 2B). These residues are highly reactive in the absence of DNA and display a 2-fold protection in its presence. Similar high reactivity is observed for peptide 219−238 that contains a number of solvent accessible residues along helix H2′ that is independent of DNA complex formation.

To summarize the data to this point, the two subdomains of the C-terminal core of *S. cerevisiae* TBP display asymmetry with regard to the •OH reactivity of residues both within the DNA-binding interface and along the top of the molecule. Of particular note is the minimal reactivity of the saddle residues of the H2 subdomain in the absence of DNA. The DNA dependence of the •OH reactivities is also asymmetric with only the H2′ subdomain saddle residues undergoing a reduction in reactivity upon formation of the TBP−DNA complex. In addition, DNA-dependent changes in •OH reactivity are observed for residues along the top of the H2 subdomain, while no changes are observed along the top of the H2′ subdomain.

Additional C-Terminal Domain Peptides. The power of footprinting, providing a plethora of separate reports on multiple sites, is also the bane of its presentation! For this reason, a subset of the data was presented in the preceding discussion in developing the pattern of •OH reactivity and its modulation by DNA binding. In this section, the remainder of the analyzed peptides of the C-terminal domain is presented. The reactive residues of peptide 80−83 are leucines that are buried within the β-sheet core of the H2 subdomain. Their low reactivity is further reduced 2-fold upon DNA binding. Proline 109 is the sole reactive residue on peptide 106−110 and is located on the top of the molecule adjacent to helix H2 (Figure 5, column 1). Its reactivity in the free protein is high, decreasing by slightly more than 3-fold in the TBP−DNA complex. F152 and F155, adjacent to helix 2, are the reactive residues of peptide 152−155. They are moderately reactive in the absence of DNA and 2-fold protected in its presence. The reactivity to oxidation of all of these topside residues of the H2 subdomain is DNA-dependent.

The final peptide analyzed (residues 212−218) contains a single reactive residue, L214, which is buried within the β-sheet core of the H2′ subdomain. Despite its "zero" solvent accessibility in both the absence and presence of DNA, this residue is oxidized by •OH (Figure 5, column 2) and 3-fold protected by DNA. We hypothesize that the reactivity of this "buried" residue reflects the dynamics of the protein molecule in solution (*46*). Studies to test this conjecture are in progress.

N-Terminal Domain Residues. The results presented above for residues located within the C-terminal domain are incompatible with the solvent accessibility predictions made from the crystal structures of the isolated C-terminal domain. We now present the data acquired for the 61 residues of the N-terminal domain for which no crystallographic structural information is available. Peptide 7−11 has only F9 as a radiolytically modifiable residue. In light of the general belief that the N-terminal domains of TBP are "unstructured", the very low reactivity of this residue [0.12 ± 0.01 s^{-1} compared with a value of $\sim$3 s^{-1} for solvent accessible phenylalanine (*45*)] is surprising given its proximity to the end of the N-terminus of the polypeptide chain. Its absence of reactivity is also independent of the binding of DNA (Table 1).

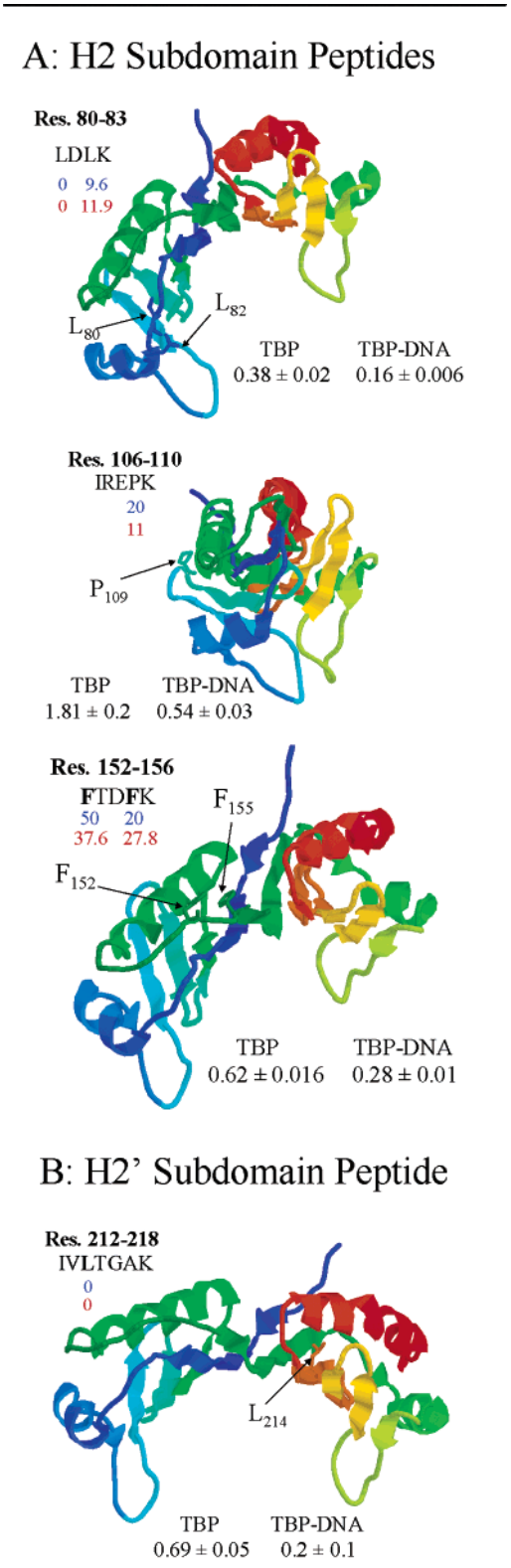

FIGURE 5: Ribbon diagram representations of the C-terminal domain of *S. cerevisiae* TBP in which radiolytically modified residues are denoted as described in the legend of Figure 2.

Peptide 16−23 contains two reactive residues, F18 and P20. The reactivity of the two residues of this peptide is greater than that of F10 and diminished by $\sim$4-fold upon formation of the TBP−DNA complex (Table 1). Peptide 24−31 contains a single modifiable residue, Trp-26, whose fluorescence has been used to probe the structure of the

Table 1: Rates of Radiolytic Modification for the Tryptic Peptides Derived from the N-Terminal Domain of *S. cerevisiae* TBP[a]

sequence	residues	rate for TBP (s^{-1})	rate for TBP−DNA (s^{-1})
LKE**F**K	7−11	0.12 ± 0.01	0.14 ± 0.01
IV**F**D**P**NTR	16−23	0.72 ± 0.03	0.15 ± 0.016
QV**W**ENQNR	24−31	3.92 ± 0.2	2.30 ± 0.13
DGT**P**ATT**F**QSEEDIKR	32−48	0.32 ± 0.02	0.78 ± 0.02
RAA**P**ESEK	49−55	not detectable	not detectable

[a] These rates are derived from data such as that shown in Figure 1.

N-terminal domain of *S. cerevisiae* TBP (*17*, *39*, *47*). This residue is reactive in the free protein and protected slightly less than 2-fold upon the binding of TBP (Table 1). Peptide 32−48 contains two modifiable residues, P36 and F40, whose low reactivity is increased approximately 2-fold in the TBP−DNA complex (Table 1). Since phenylalanine has a much higher intrinsic reactivity to •OH oxidation than proline, phenylalanine likely dominates the reactivity of peptides 16−23 and 32−48. Reactivity of P52 on peptide 49−55 was not detectable (Table 1).

These data acquired for the N-terminal domain of *S. cerevisiae* TBP suggest that this domain possesses secondary and/or tertiary structure that is dependent upon the binding of DNA by the protein. The correlation of the structural changes measured by radiolytic modification in the N- and C-terminal domains suggests their DNA-dependent interaction. Both the intrinsic fluorescence of W26 (*39*, *47*) and radiolytic footprinting (Table 1) show a change in the environment of this N-terminal residue upon formation of the TBP−DNA complex.

DISCUSSION

The central role of TBP in eukaryotic transcription has made this protein a frequent target of biological, biochemical, and biophysical studies. That this protein so central to eukaryotic cellular function possesses unusual structural and functional properties has piqued the interest of the research community. To date, the only structural information concerning a TBP N-terminal domain of more than rudimentary length has been obtained from fluorescence studies of the single tryptophan found in the N-terminal domain of *S. cerevisiae* TBP (*17*, *39*, *47*). These studies explore the solution structures of the C- and N-terminal domains and their relationship with each other using radiolytic modification of amino acid side chains. As will be elaborated below, unexpected and unusual features abound in these data obtained using a novel technique that are generally consistent with and complement the fluorescence studies (*39*).

The widely held belief that the N-terminal domains of TBP molecules are completely unstructured is not consistent with the published fluorescence (*17*, *39*, *47*) and present radiolytic modification studies of *S. cerevisiae* TBP with its 61-residue N-terminal domain. The N-terminal domain possesses several radiolytically sensitive residues, including a single phenylalanine on each of three separate peptides and the protein's single tryptophan on a fourth peptide. Very high reactivity would be expected for *all* of these residues if the domain is unstructured and/or has no contact with the C-terminal domain. Their low reactivities argue for the domain possessing tertiary structure and/or participating in interdomain interactions.

In addition, the radiolytic modification of residues within the N-terminal domain is sensitive to DNA binding. That a DNA-dependent conformational change occurs in this domain is supported by the *opposite* changes in reactivity observed for peptides 15−22 and 31−47. Together with the C-terminal domain protections that are discussed below, these data are consistent with the interaction between these two domains being dependent on DNA binding.

These data indicate that the two sides of the DNA-binding saddle of *monomeric* TBP are not equally solvent accessible in the absence of DNA (Figure 2). While the saddle residues of the H2′ subdomain are reactive in the absence of DNA and protected in its presence, those of the H2 subdomain are minimally reactive in both the absence and presence of DNA. This asymmetry is the opposite of the accessibilities predicted from the dimers of unliganded TBP present in the C-terminal domain crystal structure of *S. cerevisiae* TBP (*24*).

Could a collapse of the stirrups of the C-terminal subdomain toward the β-sheets that comprise the DNA-binding surface rationalize the radiolytic footprinting results? Arguing against this possibility is the absence of such motions in molecular dynamics simulations of solvated TBP (N. Pastor, personal communication). More directly, this structure would expected to be symmetric with both sides of the saddle being equivalently protected. Such a result is clearly not observed in the radiolytic footprinting data.

The hypothesis that we favor is that the N-terminal domain of *S. cerevisiae* TBP interacts with the C-terminal domain and binds within the saddle in the absence of DNA. Such a structure has precedent in transcriptional regulation by the Sigma(70) subunit of *E. coli* RNA polymerase (*48*) and supported by the diminished binding affinity of full-length human TBP for DNA (*31*, *32*). In addition, the N-terminal domain of *S. cerevisiae* TBP mediates formation of octamers along one self-assembly pathway (*16*, *17*) while apparently inhibiting formation of "saddle-to-saddle" dimers by another assembly pathway (*18*, *49*). Last, genetic studies of the N-terminal domain of *S. cerevisiae* TBP suggest that it regulates binding to DNA and other transcription factors via a specific surface of the C-terminal domain (*34*). These results provide compelling biological and biochemical evidence of functionally significant interactions between the two domains of TBP.

Panels A and B of Figure 6 present plausible models of interaction of the N- and C-terminal domains of *S. cerevisiae* TBP that are consistent with the DNA-dependent changes observed by fluorescence (*39*) and radiolytic footprinting. The structure of the C-terminal domain is assumed to be independent of DNA binding in this model, based upon the published crystallographic and biochemical studies. N-terminal domain secondary structure is not included since experimental data addressing this structural characteristic are lacking. Critically distinguishing between N-terminal conformational change and interdomain interaction will be achieved by radiolytic protein footprinting studies of the isolated domains. However, these experiments are complicated by the different self-association properties of the isolated C-terminal domain (M. Fried, personal communica-

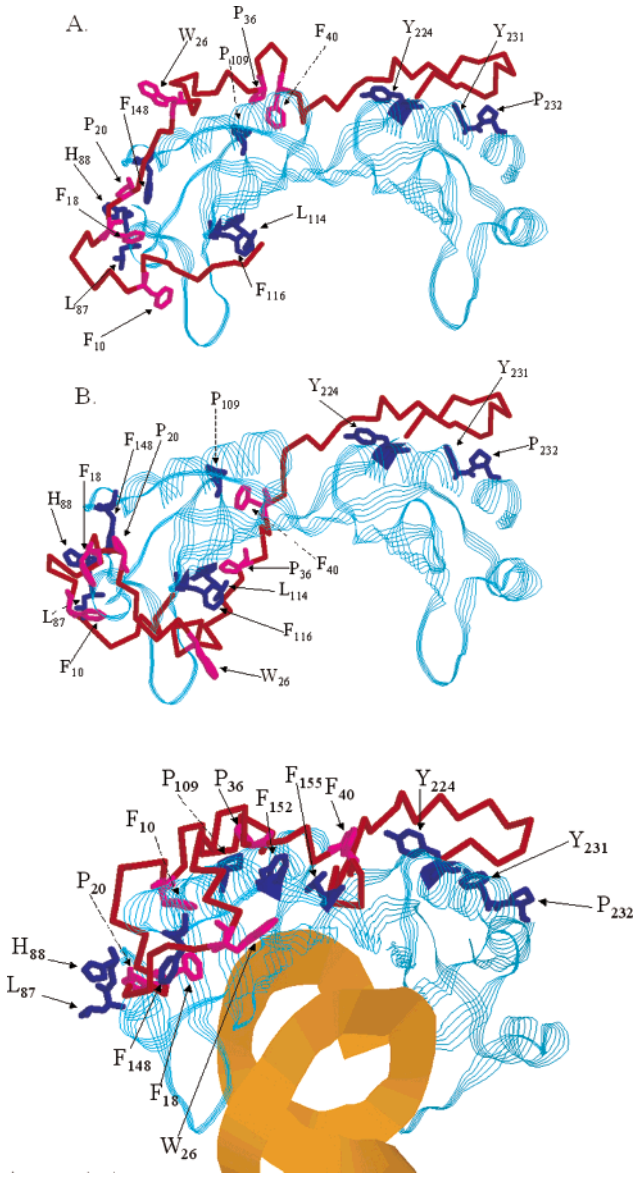

FIGURE 6: Models of plausible dockings of the N- and C-terminal domains consistent with the radiolytic modification data. The C-terminal domain is shown in blue. The N-terminal domain is shown in red. The side chains of the radiolytically sensitive residues are displayed. These models do not reflect the molecular details of the interdomain interactions but rather present a visualization of the available structural information for plausible topologies as a guide to future experiments. Panels A and B represent two dockings of the N-terminal domain that are consistent with the radiolytic modification data. Panel C shows a model for the DNA-bound protein.

tion; *18*) under these experimental conditions. Experiments designed to overcome these complications are in progress.

Models of Interdomain Interaction in the Absence of DNA. We will begin our presentation of the models at the covalent connection between the two domains and proceed toward the N-terminus of the *S. cerevisiae* TBP polypeptide. Detectable radiolytic reactivity was not observed for P52, the sole susceptible residue of peptide 49−55 (Table 1). On helix H2′ of the C-terminal domain, the fluorescence anisotropy of Y224 and Y231 is high, and these residues have low accessibility to a neutral quencher (*39*). Neither the radiolytic reactivity of peptide 49−55 nor the fluorescence parameters of Y224 and Y231 (*39*) change upon binding of TBP to DNA. Together, these results suggest that the final segment of the N-terminal polypeptide overlays the top of the H2′ subdomain and that its position does not vary upon formation of the TBP−DNA complex. Geometric considerations suggest that the N-terminal domain follows a hairpin trajectory and loops back toward the H2 subdomain (Figure 6).

Unfortunately, the reactive residues of helix H2′ are all within peptide 219−238, precluding analysis of their individual reactivities at this time (Figure 2B). While the overall reactivity of this peptide is high, this reactivity could be due to the high solvent accessibility of even a single residue. Thus, more precise positioning of the N-terminal polypeptide on top of the H2′ subdomain will await more refined analysis of the reactive residues of this peptide. Residues 55−64 of the N-terminal domain are necessary and sufficient for rescuing the viability of otherwise lethal point mutations in the C-terminal domain of TBP (*34*). We suggest that this length of polypeptide contributes to the stability, structure, and/or dynamics of the C-terminal domain structure through its interaction overlaying the H2′ helix.

The ability of protein footprinting to detect solvent accessible residues and the direct correlation between the rate of reactivity and solvent accessibility as calculated from crystallographic data have been established in published studies of lysozyme (*45*), gelsolin segment-1 (*50*), cofilin (*38*), and full-length gelsolin (*51*). The high reactivity of peptide 168−171 bearing F167 as well as peptide 202−211 bearing F207, both within H2′, highlights the solvent accessibility of the susceptible residues within these peptides on this side of the DNA-binding saddle (Figure 2B). In particular, the modification rates of 3.9 and 3.4 s^{-1} are comparable to that obtained for a single phenylalanine residue of comparable accessibility in hen egg lysozyme (*45*). However, one peptide within H2′, residues 183−195 (Figure 2), has a modification rate lower than that expected from the crystallographic data (0.86 s^{-1}). This may suggest some small differences in the structure of this region compared to the accessibilities predicted from the crystal structure. Since footprinting reports the solution structure, variations from results predicted from crystallography should occasionally be expected. Nevertheless, the higher reactivity of many residues within H2′ (including peptide 183−195) compared to the low reactivity of the symmetry-related counterparts in the H2 subdomain (Figure 2A) justify the proposed topology described below of the N-terminal domain continuing across the top of the H2′ subdomain to the H2 subdomain.

The low reactivity of F40 of the N-terminal domain places this region of the polypeptide in the proximity of the C-terminal domain (Table 1). The high reactivity of P109 along one side of helix H2 is in contrast to the lower reactivity of the peptide bearing F152 and F155 on the opposite side of this helix (Figure 5). Together, these data suggest that the N-terminal polypeptide lies along the latter side of the H2 helix (Figure 6). The observation from genetic studies that mutation of F152 and F155 confers N-terminal domain dependence on cell viability further implicates these radiolytically protected residues in interdomain interactions (*34*).

At this point in the N-terminal polypeptide sequence, the radiolytic modification data are consistent with two different topologies relative to the C-terminal domain. In one topology,

the N-terminal polypeptide lays across the top surface of the C-terminal domain adjacent to the H2 helix (Figure 6A). The protection of F18 and F10 further down the polypeptide chain is proposed to arise from interactions with H88 and L87 on the "end" of the C-terminal domain and F116 and L114 within the saddle of the H2′ subdomain, respectively. In the second topology, the N-terminal polypeptide interacts with the saddle, protecting F116 and L114 from modification. The protections of F18 and F10 further down the polypeptide chain are modeled to protect H88 and L87 on the end of the C-terminal domain (Figure 6B).

Both of the proposed topologies place the single tryptophan of *S. cerevisiae* TBP, W26, in solvent-exposed positions consistent with its high rate of radiolytic modification. At first glance, this conclusion is inconsistent with this residue's nonpolar environment as follows from its fluorescent properties (*39*). However, effective radiolytic modification of tryptophan would occur if only a "tip" of the aromatic ring were transiently solvent exposed because of the dynamics of the molecule in solution. Thus, further studies will be required to quantitatively relate the structures predicted from fluorescence and radiolytic modification. Overall, the radiolytic footprinting data show that the N-terminal domain has structure, interacts with the C-terminal domain, and protects it from solvent residues within the H2 side of the DNA-binding saddle.

Allosteric Regulation of Interdomain Interactions by DNA Binding. After DNA binds, the reactivities of the H2 subdomain residues L87 and H88 on the "side" of the H2 subdomain increase significantly while residues L80, L82, P109, F148, F152, and F155 along the "top" are protected compared to their reactivity in free TBP (Figures 2A and 5A). In contrast, little change in radiolytic reactivity as a function of DNA binding is observed for the residues of and around helix H2′. A maximum 2-fold level of protection of F168 and P169 in this subdomain is observed upon DNA binding (Figure 2B). In addition, the last radiolytically sensitive residue of the N-terminal domain prior to the polypeptide chain entering the C-terminal domain is not reactive in either the absence or presence of bound DNA. This latter result contrasts with the increased reactivity of peptide 32−48 (Table 1), a portion of the N-terminal domain that is hypothesized to interact with the H2 helix (Figure 6A,B).

Taken together, these data suggest a shift in the position of the N-terminal domain along the upper surface of the C-terminal domain around the H2 helix upon DNA binding with a more localized conformational change around the H2′ subdomain (Figure 6C). We hypothesize that these changes in the interdomain interaction are coupled to the displacement of the N-terminal domain from interaction with residues with the DNA-binding saddle upon DNA binding. The lower reactivity of residues in the H2 subdomain suggests that the N-terminal domain might form a folded structure in the DNA complex on top of helix H2 and β-sheet S1 in monomeric TBP. Consistent with this proposal, studies of W26 fluorescence demonstrated an increase in the correlation time of the N-terminal domain as a result of more intimate association with the C-terminal domain in the DNA complex (*39*). This model suggests that the N-terminal domain could potentially play a role in the binding of other transcription factors to the top surface of TBP (*28*, *52*, *53*).

Functional Implications for DNA Binding. The sequence specific binding of TBP to DNA is considered a defining example of "indirect readout" in which macromolecular structure and conformational accommodation are the key elements of molecular recognition. The large distortion of the DNA and the modest changes of the structure of the C-terminal domain of TBP observed within the cocrystal structures (*5*, *54*) have suggested DNA conformational change as the dominant contribution to the indirect readout mechanism. These data suggest that interdomain interactions play an active role in the formation of the TBP−DNA complex.

This study is the first solution analysis of the structure of TBP in which the asymmetrical structure of the "saddle" surface responsible for interaction with DNA has been shown. This structural asymmetry comes from the N-terminal domain having different conformations when free or bound to DNA. While free, the N-terminal domain interacts with the "H2 subdomain" half of the C-domain of TBP screening this portion of the saddle from DNA. When bound, the N-terminal domain of TBP changes its position relative to the C-domain and converts the DNA interacting saddle to the symmetrical structure visible in the crystal.

The conformational adjustment of TBP upon binding to DNA can have some structural and functional consequences. TBP displays unusually slow association and dissociation kinetics (*55*). The slow rate of association has been shown to result from the inefficient formation of a stable TBP−DNA complex from the initial encounter complex (*41*, *56*, *57*). Genetic and biochemical studies have shown significant N-terminal domain-mediated autoinhibition of DNA binding for human TBP (*31*, *32*). The radiolytic footprinting and kinetics data can be interpreted to reflect "autoinhibition" of DNA binding by the N-terminal domain of *S. cerevisiae* TBP, although the interdomain interaction is clearly more labile in the yeast protein. In this view, an equilibrium between a "docked" and "undocked" N-terminal domain on the C-terminal core would affect the probability that the initial encounter complex would be productive and allow the protein to proceed down the DNA binding pathway. Screening of one side of the C-domain saddle with the N-domain makes interaction of the C-domain with DNA difficult and rationalizes destabilization of the complex of DNA with native TBP as compared with its N-truncated variant (*31*).

In addition, TBP binds with preferred polarity within the transcription preinitiation complexes that dictate the direction of transcription initiation (*58*). The mechanisms by which the efficient assembly of appropriately directional preinitiation complexes is achieved remain uncertain. Most of the amino acids that contact DNA are identical in the two halves of the C-domain (*24*, *54*). Theory (*58*) and experiment (*59*) agree that TBP can bind DNA asymmetric TATA box sequences with roughly equivalent affinity despite the presence of one orientation in the TBP−DNA cocrystals whose structures have been determined (*7*, *58*, *60*). Both structural (*7*) and kinetic (*61*) hypotheses have been proposed to define the preferred orientation of the C-domain of TBP and DNA within the complex, a process that clearly involves the participation of other general transcription factors (*59*). The asymmetry of the DNA-binding saddle of full-length *S. cerevisiae* TBP in solution conferred by interaction with the

N-terminal domain revealed in this study provides an avenue by which the symmetry of TBP−TATA box interactions can be influenced. The changes in the structure of TBP upon binding to DNA observed in this and complementary fluorescence (*39*) studies similarly provide an underlying mechanism for the allosteric regulation of preinitiation complex assembly on promoters.

Protein Footprinting of Protein−DNA Complexes. In conclusion, these results also demonstrate that the X-ray radiolytic modification footprinting method can be utilized successfully to study the protein in a protein−nucleotide complex in a fashion complementary to similar studies from the DNA point of view (*42*, *62*). Assaying radiolytic modification of proteins is complementary to assaying hydroxyl radical cleavage. In cleavage approaches, proteins are end labeled and subjected to cleavage by the application of hydroxyl radicals generated using Fenton reagents (*63*, *64*). Attack of the backbone C_α−H bonds by hydroxyl radicals can lead to strand cleavage, although at rates far slower than the rates of oxidative modifications (*36*). The peptide fragments are sorted by size by SDS−PAGE, and a "footprint" is discerned by decreased intensity of fragment bands corresponding to sites of solvent inaccessibility in a manner comparable to nucleic acid footprinting, albeit with limited fragment length resolution. In contrast, the analysis by mass spectrometry of the sites of modification allows quantitation through the determination of the rates of reactivity. In addition, as is the case for TBP, highly reactive aromatic side chain residues of proteins are often at ligand binding and macromolecular interaction interfaces. Thus, the use of mass spectrometry to analyze the oxidative products of radiolytic modification provides a highly specific probe of such sites. Improvements in the mass spectrometry techniques applied to radiolytic footprinting, including the use of tandem MS techniques (*37*), will further enhance the resolution and applicability of this protein footprinting technique.

ACKNOWLEDGMENT

We thank Ms. Elizabeth Jamison for preparing the TBP used in these studies and Michael Sullivan, John Toomey, and Narcisse Komas for their support of experimental studies conducted at NSLS beamline X-28C.

REFERENCES

1. McKnight, S. L. (1996) *Genes Dev. 10*, 367−381.
2. Burley, S. K. (1996) *Curr. Opin. Struct. Biol. 6*, 69−75.
3. Kim, J. L., Nikolov, D. B., and Burley, S. K. (1993) *Nature 365*, 520−527.
4. Kim, Y., Geiger, J. H., Hahn, S., and Sigler, P. B. (1993) *Nature 365*, 512−520.
5. Kim, J. L., and Burley, S. K. (1994) *Nat. Struct. Biol. 1*, 638−653.
6. Juo, Z. S., Chiu, T. K., Leiberman, P. M., Baikalov, I., Berk, A. J., and Dickerson, R. E. (1996) *J. Mol. Biol. 261*, 239−254.
7. Nikolov, D. B., Chen, H., Halay, E. D., Hoffman, A., Roeder, R. G., and Burley, S. K. (1996) *Proc. Natl. Acad. Sci. U.S.A. 93*, 4862−4867.
8. Patikoglou, G. A., Kim, J. L., Sun, L., Yang, S. H., Kodadek, T., and Burley, S. K. (1999) *Genes Dev. 13*, 3217−3230.
9. Wu, J., Parkhurst, K. M., Powell, R. M., Brenowitz, M., and Parkhurst, L. J. (2001) *J. Biol. Chem. 276*, 14614−14622.
10. Starr, D. B., Hoopes, B. C., and Hawley, D. K. (1995) *J. Mol. Biol. 250*, 434−446.
11. Bareket-Samish, A., Cohen, I., and Haran, T. E. (2000) *J. Mol. Biol. 299*, 965−977.
12. Wu, J., Parkhurst, K. M., Powell, R. M., and Parkhurst, L. J. (2001) *J. Biol. Chem. 276*, 14623−14627.
13. Paule, M. R., and White, R. J. (2000) *Nucleic Acids Res. 28*, 1283−1298.
14. Roeder, R. G. (1996) *Trends Biochem. Sci. 21*, 327−335.
15. Geiduschek, E. P., and Kassavetis, G. A. (2001) *J. Mol. Biol. 310*, 1−26.
16. Daugherty, M. A., Brenowitz, M., and Fried, M. G. (1999) *J. Mol. Biol. 285*, 1389−1399.
17. Daugherty, M. A., Brenowitz, M., and Fried, M. G. (2000) *Biochemistry 39*, 4869−4880.
18. Campbell, K. M., Ranallo, R. T., Stargell, L. A., and Lumb, K. J. (2000) *Biochemistry 39*, 2633−2638.
19. Coleman, R. A., Taggart, A. K., Benjamin, L. R., and Pugh, B. F. (1995) *J. Biol. Chem. 270*, 13842−13849.
20. Horikoshi, M., Yamamoto, T., Ohkuma, Y., Weil, P. A., and Roeder, R. G. (1990) *Cell 61*, 1171−1178.
21. Lieberman, P. M., Schmidt, M. C., Kao, C. C., and Berk, A. J. (1991) *Mol. Cell. Biol. 11*, 63−74.
22. Burley, S. K., and Roeder, R. G. (1996) *Annu. Rev. Biochem. 65*, 769−799.
23. Nikolov, D. B., and Burley, S. K. (1994) *Nat. Struct. Biol. 1*, 621−637.
24. Chasman, D. I., Flaherty, K. M., Sharp, P. A., and Kornberg, R. D. (1993) *Proc. Natl. Acad. Sci. U.S.A. 90*, 8174−8178.
25. Nikolov, D. B., Chen, H., Halay, E. D., Usheva, A. A., Hisatake, K., Lee, D. K., Roeder, R. G., and Burley, S. K. (1995) *Nature 377*, 119−128.
26. Littlefield, O., Korkhin, Y., and Sigler, P. B. (1999) *Proc. Natl. Acad. Sci. U.S.A. 96*, 13668−13673.
27. Geiger, J. H., Hahn, S., Lee, S., and Sigler, P. B. (1996) *Science 272*, 830−836.
28. Kamada, K., Shu, F., Chen, H., Malik, S., Stelzer, G., Roeder, R. G., Meisterernst, M., and Burley, S. K. (2001) *Cell 106*, 71−81.
29. Lescure, A., Lutz, Y., Eberhard, D., Jacq, X., Krol, A., Grummt, I., Davidson, I., Chambon, P., and Tora, L. (1994) *EMBO J. 13*, 1166−1175.
30. Das, D., and Scovell, W. M. (2001) *J. Biol. Chem. 276*, 32597−32605.
31. Mittal, V., and Hernandez, N. (1997) *Science 275*, 1136−1140.
32. Zhao, X., and Herr, W. (2002) *Cell 108*, 615−627.
33. Kuddus, R., and Schmidt, M. C. (1993) *Nucleic Acids Res. 21*, 1789−1796.
34. Lee, M., and Struhl, K. (2001) *Genetics 158*, 87−93.
35. Maleknia, S. D., Brenowitz, M., and Chance, M. R. (1999) *Anal. Chem. 71*, 3965−3973.
36. Maleknia, S. D., Ralston, C. Y., Brenowitz, M. D., Downard, K. M., and Chance, M. R. (2001) *Anal. Biochem. 289*, 103−115.
37. Chance, M. R. (2001) *Biochem. Biophys. Res. Commun. 287*, 614−621.
38. Guan, J. Q., Vorobiev, S., Almo, S. C., and Chance, M. R. (2002) *Biochemistry 41*, 5765−5775.
39. Khrapunov, S., Pastor, N., and Brenowitz, M. (2002) *Biochemistry 41*, 9559−9571.
40. Petri, V., Hsieh, M., and Brenowitz, M. (1995) *Biochemistry 34*, 9977−9984.
41. Parkhurst, K. M., Brenowitz, M., and Parkhurst, L. J. (1996) *Biochemistry 35*, 7459−7465.
42. Dhavan, G. M., Chance, M. R., and Brenowitz, M. (2003) in *Analysis of Macromolecules: A Practical Approach* (Johnson, K. A., Ed.) IRL Press at Oxford University Press, Oxford, U.K. (in press).
43. Ralston, C. Y., Sclavi, B., Sullivan, M., Deras, M. L., Woodson, S. A., Chance, M. R., and Brenowitz, M. (2000) *Methods Enzymol. 317*, 353−368.
44. Sclavi, B., Woodson, S., Sullivan, M., Chance, M., and Brenowitz, M. (1998) *Methods Enzymol. 295*, 379−402.
45. Kiselar, J. G., Maleknia, S. D., Sullivan, M., Downard, K. M., and Chance, M. R. (2002) *Int. J. Radiat. Biol. 78*, 101−114.
46. Pastor, N., Weinstein, H., Jamison, E., and Brenowitz, M. (2000) *J. Mol. Biol. 304*, 55−68.
47. Perez-Howard, G. M., Weil, P. A., and Beechem, J. M. (1995) *Biochemistry 34*, 8005−8017.
48. Dombroski, A. J., Walter, W. A., and Gross, C. A. (1993) *Genes Dev. 7*, 2446−2455.
49. Jackson-Fisher, A. J., Chitikila, C., Mitra, M., and Pugh, B. F. (1999) *Mol. Cell 3*, 717−727.

50. Goldsmith, S. C., Guan, J. Q., Almo, S., and Chance, M. (2001) *J. Biomol. Struct. Dyn. 19*, 405−418.
51. Kiselar, J. G., Janmey, P., Almo, S., and Chance, M. R. (2003) *Proc. Natl. Acad. Sci. U.S.A.* (in press).
52. Cang, Y., Auble, D. T., and Prelich, G. (1999) *EMBO J. 18*, 6662−6671.
53. Dasgupta, A., Darst, R. P., Martin, K. J., Afshari, C. A., and Auble, D. T. (2002) *Proc. Natl. Acad. Sci. U.S.A.* (in press).
54. Kim, Y. C., Geiger, J. H., Hahn, S., and Sigler, P. B. (1993) *Nature 365*, 512−520.
55. Hoopes, B. C., LeBlanc, J. F., and Hawley, D. K. (1992) *J. Biol. Chem. 267*, 11539−11547.
56. Parkhurst, K. M., Richards, R. M., Brenowitz, M., and Parkhurst, L. J. (1999) *J. Mol. Biol. 289*, 1327−1341.
57. Powell, R. M., Parkhurst, K. M., Brenowitz, M., and Parkhurst, L. J. (2001) *J. Biol. Chem. 276*, 29782−29791.
58. Miaskiewicz, K., and Ornstein, R. L. (1996) *J. Biomol. Struct. Dyn. 13*, 593−600.
59. Cox, J. M., Hayward, M. M., Sanchez, J. F., Gegnas, L. D., van der Zee, S., Dennis, J. H., Sigler, P. B., and Schepartz, A. (1997) *Proc. Natl. Acad. Sci. U.S.A. 94*, 13475−13480.
60. Kim, J. L., Nikilov, D. B., and Burley, S. K. (1993) *Nature 365*, 520−527.
61. Liu, Y., and Schepartz, A. (2001) *Biochemistry 40*, 6257−6266.
62. Dhavan, G. M., Crothers, D. M., Chance, M. R., and Brenowitz, M. (2002) *J. Mol. Biol. 315*, 1027−1037.
63. Baichoo, N., and Heyduk, T. (1997) *Biochemistry 36*, 10830−10836.
64. Heyduk, E., and Heyduk, T. (1994) *Biochemistry 33*, 9643−9650.

BI027203F